16th ICAAR LISBOA 2020-2022

16th International Conference on
Alkali-Aggregate Reaction in Concrete
Lisboa | LNEC | Portugal | 31 May - 2 June 2022

http://icaar2020-2022.lnec.pt

A micro-XAS and XRD study of the crystalline alkali-silica reaction products

Guoqing Geng [(1) (2)], Zhenguo Shi [(3)], Barbara Lothenbach [(4)], Andreas Leemann [(5)], Erich Wieland [(6)], Rainer Dähn [(7)]

(1) National University of Singapore, Department of Civil and Environmental Engineering, Singapore 117576, ceegg@nus.edu.sg.

(2) Laboratory for Waste Management, Paul Scherrer Institut, 5232 Villigen PSI, Switzerland.

(3) Laboratory for Concrete & Construction Chemistry, Swiss Federal Laboratories for Materials Science and Technology (Empa), 8600 Dübendorf, Switzerland, Zhenguo.Shi@empa.ch.

(4) Laboratory for Concrete & Construction Chemistry, Swiss Federal Laboratories for Materials Science and Technology (Empa), 8600 Dübendorf, Switzerland, Barbara.Lothenbach@empa.ch.

(5) Laboratory for Concrete & Construction Chemistry, Swiss Federal Laboratories for Materials Science and Technology (Empa), 8600 Dübendorf, Switzerland, Andreas.Leemann@empa.ch.

(6) Laboratory for Waste Management, Paul Scherrer Institut, 5232 Villigen PSI, Switzerland, erich.wieland@psi.ch

(7) Laboratory for Waste Management, Paul Scherrer Institut, 5232 Villigen PSI, Switzerland, rainer.daehn@psi.ch.

Abstract

Deterioration induced by alkali silica reaction (ASR) significantly shortens the service life of worldwide concrete infrastructure. Increasing micro-morphological evidences have unveiled the nano-platy morphology of the reaction product inside the aggregate, indicating its crystalline nature in contrast to the amorphous ASR product observed adjacent to the interface between aggregate and cement paste. However, the crystal structure and the property of this crystalline ASR product have not been sufficiently investigated. Using synchrotron-based micro X-ray absorption spectroscopy (micro-XAS), we demonstrated that the chemical environment of K and Ca in the crystalline ASR products resembles that in the natural mineral shlykovite. Their structural similarity is further validated by the comparable X-ray diffraction data. Via high pressure XRD (HP-XRD) measurement, we have determined the anisotropic incompressibility of the crystalline ASR products, as well as their bulk modulus. The results provide fundamental input for understanding the formation of the ASR product, and for multi-scale mechanical modeling of the damage process.

***Keywords**: alkali-silica reaction; bulk modulus; crystalline; micro-XAS; XRD*

1. BACKGROUND

Concrete degradation due to long-term physiochemical process is ubiquitous worldwide. Among them, one of the most deteriorating processes is alkali-silica-reaction (ASR). It happens between the siliceous component of aggregate and the alkaline pore solution of concrete. The reaction product, bearing the composition of calcium-alkali silicate hydrate, is considered to be the source of an expansion stress that leads to internal cracking of concrete. A wide variety of structures, e.g. supporting walls, bridges or dams can be affected, which raises critical safety concern and cost for repair/rebuild. In a preliminary survey, in Switzerland over 400 affected structures were identified and it is expected that several alpine dams have to be repaired or rebuilt in the coming years [1].

For many decades the ASR product has been considered mainly as an amorphous gel. The source of the expansion has also been considered due to volumetric swelling of the ASR gel when in contact with moisture. However in the recent years increasing amount of morphological data at the microscale have shown that the ASR product often exhibits nano-crystallinity in the product vein inside the reacted aggregates [2]-[5]. Since the aggregate is the origin of the expansion, it becomes doubtful whether the 'gel expansion' hypothesis is able to describe the real mechanism of ASR damage. It is crucial to understand whether and how the nano-crystalline ASR products swell, in order to fully understand the ASR damage process.

To answer this question, the chemistry and molecular structure of the ASR product have to be clarified first. Researchers have investigated the crystalline ASR products from affected concrete using XRD and SEM-EDX. Several mineralogical analogues have been proposed, including okenite ($CaSi_2O_5 \cdot 2H_2O$) [6], mountainite ($KNa_2Ca_2[Si_8O_{19}(OH)] \cdot 6H_2O$) [3], rhodesite ($KHCa_2[Si_8O_{19}] \cdot 5H_2O$) [3], and the solid solution between mountainite, shlykovite ($KCa[Si_4O_9(OH)] \cdot 3H_2O$) and fedorite ($(K,Na)_{2.5}(Ca,Na)_7[Si_{16}O_{38}(OH,F)_2] \cdot 3.5H_2O$) [7]. As shown in Figure 1.1a, okenite has a rather thick main layer, composed of three silicate sheets and two Ca layers. The interlayer of okenite hosts Ca in coordination of water molecules. Mountainite (Figure 1.1b) and shlykovite (Figure 1.1c) have more configurational similarity. Their main layers are both Ca and charge-balanced by two silicate sheets. K in mountainite co-exist with Ca in the main layer, whereas K in shlykovite is in the silicate layer. Na is hosted in the interlayer of mountainite, yet it is not reported in the structure of natural shlykovite. SEM-EDX data have confirmed that the presence of alkali (Na/K) in crystalline ASR product [8], suggesting the okenite structure is less likely an analogue of the crystalline ASR product. While the mountainite family, e.g. mountainite and shlykovite, is a more plausible answer, as also confirmed by a recent micro-XRD study [9]. More unambiguous evidences are needed to further validate the similarity of the ASR products, both amorphous and crystalline, with the mountainite family minerals.

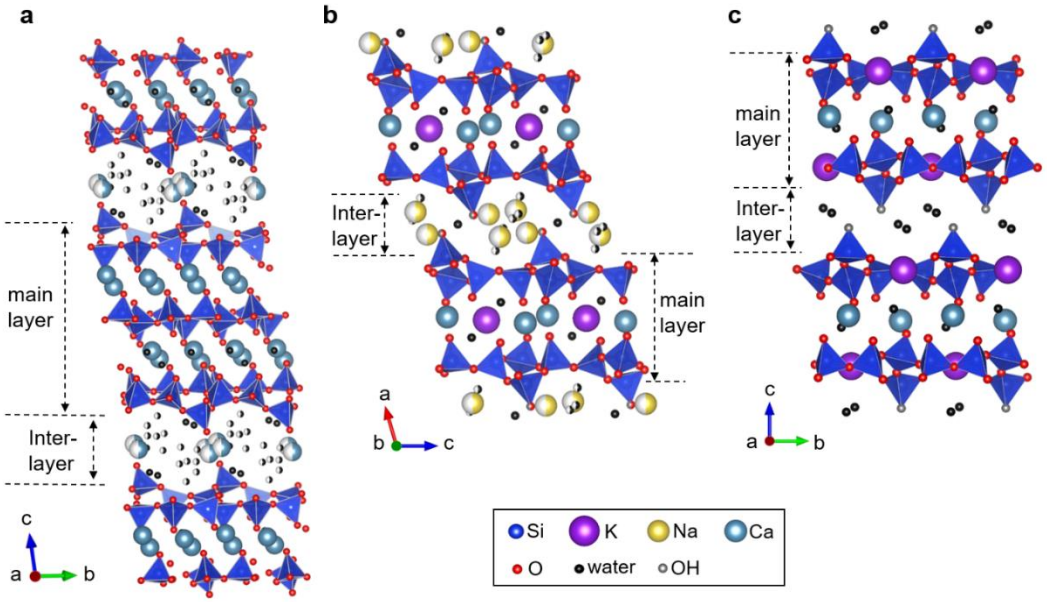

Figure 1.1: Crystal structures of (a) okenite, (b) mountainite and (c) shlykovite. Spheres partially of white color indicate partial occupancy. Note that the view of (c) is along [100] so that the layer stacks vertically, similarly as in (a) and (b). The figures are adapted from [14].

In an ongoing project funded by the Swiss National Science Foundation, ASR products are both synthesized in laboratory and collected on-site from affected concrete. Systematic investigations were conducted to decipher the atomistic scale structure of both crystalline and amorphous ASR products, the thermodynamic data of the reaction system, and the multiscale structural and mechanical evolution. In this conference paper, we aim to summarize the key findings of the atomistic configuration of the ASR product collected from affected concrete, as well as the mechanical behavior of the crystalline ASR product under compression loading. The work here has involved intensive usage of the synchrotron-based methods, including X-ray absorption spectroscopy and X-ray diffraction at ambient and high pressure.

2. METHODOLOGY

2.1 Sample preparation

Four affected concrete from the field were studied. 'Mels1' is from the abutment of a 50-year-old bridge in Mels, Switzerland. 'ES1' and 'ES2' are from concrete cubes exposed for 14 years to natural conditions in Valencia (Spain) and Milan (Italy), respectively [10]. 'N1' was obtained from a concrete subjected to Norwegian 38 °C prism test for two years. Extractions from these concrete were dried at 50 °C for three days, impregnated with epoxy and polished for the micro-XAS characterization. The thin-sections were then carbon-coated and studied with SEM-EDX.

Three powders of the crystalline ASR products from the affected concrete were carefully extracted. Sample 'Mels_pore' was extracted from a pore near an aggregate surface in Mels_1. Sample 'ES1_agg' and 'ES1_pore' were extracted from an aggregate and from a pore in ES1, respectively. The extracted powders were sealed in plastic vials immediately after extraction.

Natural minerals and lab-synthesized samples were studied as references. Mountainite and shlykovite were obtained from a Russian mineralogist [11]. Lab-synthesized ASR samples were prepared by mixing SiO_2, CaO, (Na/K)OH and water in certain stoichiometry and kept at 80 ℃ for nearly three months. Two of the obtained samples, namely SKC and SNC, were studied because their crystal structure highly resembles that of shlykovite [12]. A calcium-silicate-hydrates (C-S-H) sample with significant K-uptake was also studied, hereafter named K_CSH. The general information of all studied samples are summarized in Table 2.1.

Table 2.1: Sources and chemical compositions of the studied samples. The water content (*m*) is unclear for some samples.

Sample	Source	Composition	
Mountainite	Natural	$Na_{0.25}K_{0.125}Ca_{0.25}SiO_{2.375}(OH)_{0.125}$•0.75 H_2O	
Shlykovite	Natural	$K_{0.25}Ca_{0.25}SiO_{2.25}(OH)_{0.25}$•0.75 H_2O	
SKC	Lab synthetic	$K_{0.25}Ca_{0.25}SiO_{2.38}$•0.88 H_2O	
SNC	Lab synthetic	$Na_{0.25}Ca_{0.25}SiO_{2.38}$•0.95 H_2O	
K_CSH	Lab synthetic	$K_{0.17}Ca_{0.30}SiO_{2.385}$•$mH_2O$	
Mels1	Core from a Swiss Bridge	Crystalline	$Na_{0.07}K_{0.16}Ca_{0.22}SiO_{2.335}$•$mH_2O$
ES1	Concrete cube, Valencia	Crystalline	$Na_{0.11}K_{0.2}Ca_{0.24}SiO_{2.395}$•$mH_2O$
		Amorphous	$Na_{0.09}K_{0.15}Ca_{0.61}SiO_{2.73}$•$mH_2O$
ES2	Concrete cube, Milan	Crystalline	$Na_{0.08}K_{0.19}Ca_{0.24}SiO_{2.375}$•$mH_2O$
		Amorphous	$Na_{0.14}K_{0.16}Ca_{0.31}SiO_{2.46}$•$mH_2O$
N1	Norwegian 38 °C prism test	Crystalline	$Na_{0.08}K_{0.18}Ca_{0.22}SiO_{2.35}$•$mH_2O$
		Amorphous	$Na_{0.07}K_{0.15}Ca_{0.39}SiO_{2.4}$•$mH_2O$

2.2 SEM-EDX

A *FEI Quanta 650* SEM was used at 12 kV and 120 μA to study the micro-morphology of the thin-sections. A coupled EDS was used to probe the chemical compositions. For each thin-section, 10-30 EDS measurements were collected near the measured points in micro-XAS. The chemical compositions of the ASR products are shown in Table 1.

2.3 Micro-XAS

Micro-XAS study was conducted at the PHOENIX beamline of the Swiss Light Source, which operates in the energy range from 0.3-8 keV. The beam can be focused as small as 3 by 3 μm^2. Thin-sections were mounted on a sample stage in the vacuum chamber, together with powder samples (mountainite, shlykovite, SKC, SNC and K_CSH) that were spread on a copper plate. The fluorescence signal was collected with an incident beam energy of 4050 eV. The element mappings were compared with SEM images to identity the crystalline and amorphous product regions. At the points of interest, the incident beam energy was scanned to obtain the XAS at Ca, K and Na *K*-edge. The spectra were normalized and processed using the Athena package.

2.4 High-pressure XRD

The powder samples extracted from affected concrete, i.e Mels_pore, ES1_pore, ES1_agg, were investigated by high-pressure XRD at beamline P02.2 of the Deutsches Elektronen-Synchrotron (DESY, Hamburg, Germany). An incident energy of 25.45 keV (wavelength λ=0.4872 Å) was used. Raw diffraction data were recorded with a PE-XRD1621 image plate. A 250-µm-thick stainless steel was pre-indented to 70-90 µm thick, where a cylindrical hole (diameter 150-200 µm) was created by laser drilling. The powder samples were carefully loaded to these holes (sample chambers). A diamond anvil cell was used to create hydrostatic pressure, using a solution of ethanol and methanol (volume ratio 4:1) as the pressure medium. The pressure was increased from ambient condition to 8-10 GPa, at a step size of 1-2 GPa, followed by an unloading. Small quantities of ruby (Cr-doped Al_2O_3) was also loaded in the sample chamber, whose fluorescence signal was measured to calibrate the applied hydrostatic pressure. The 2D diffraction images were recorded at each pressure value, and then processed with *Dioptas* to yield the 1D diffractogram. Diffraction of CeO_2 powder was measured to calibrate the center of the beam on the detector and the sample-to-detector distance.

3. RESULTS AND DISCUSSIONS

3.1 Chemical environment probed by micro-XAS

A representative micro-chemistry study of ES2 is shown in Figure 3.1. An ASR product vein runs from inside the aggregate (right side of Figure 2a) towards the hardened cement paste (left side of Figure 3.1a), with its morphology changing from nano-crystalline to amorphous. A potassium fluorescence mapping (Figure 3.1b) indicates that the concentration of K in the crystalline product region is clearly higher than the less-crystalline product, which is closer to the cement paste. Such a contrast on K-mapping enables the selective measurement of spots with different morphology.

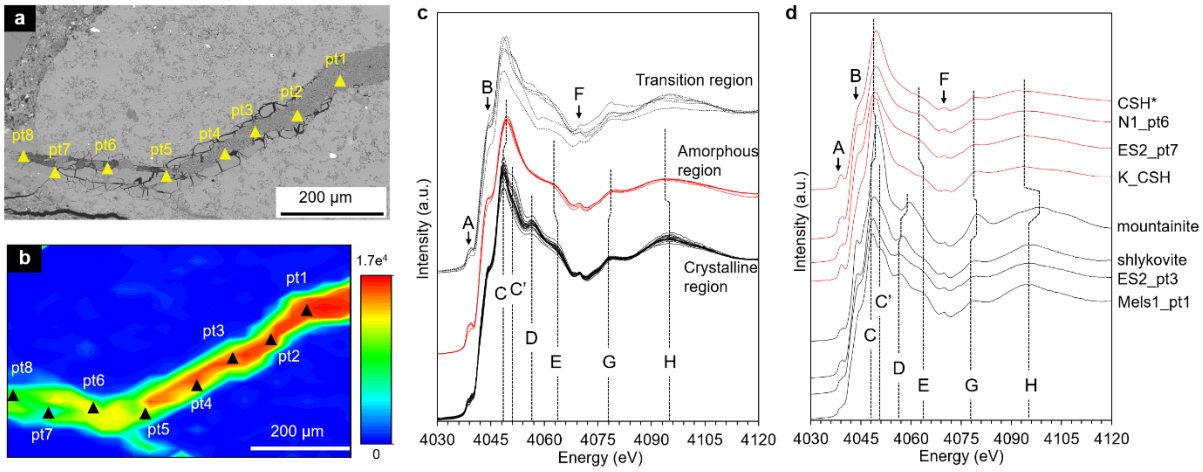

Figure 3.1: An SEM (a) and potassium fluorescence (b) images of the ASR product vein in sample ES2. The Ca *K*-edge XAS of all measured points on the thin-sections (c), compared with the spectra of reference phases (d). The figures are adapted from [14].

In the area of interest, eight points were selected from inside the aggregate towards the hardened cement paste domain (pt1 to pt8 in Figure 3.1a & 3.1b). Each point was subject to micro-XAS measurements. The XAS result near the Ca *K*-edge is shown in Figure 3.1c, together with the data from the other three thin-section samples from various field sources. The Ca *K*-edge spectra have abundant features, including 6-8 clearly resolved peaks (Figure 3.1c). Based on the location, shape and the number of peaks, all the obtained spectra can be grouped into three categories: the spectra of the crystalline region, the amorphous region and the transition region between them. Despite the distinct sources, the spectra of the crystalline ASR products are highly comparable; the spectra of the amorphous regions are also nearly identical. This indicates a similarity in crystal structure of the crystalline ASR products from four different field sources, as well as a similarity of the amorphous ASR product with all field samples. Meanwhile, the spectra of the crystalline and amorphous ASR are clearly different from each other. There is a shift of 0.3-0.6 eV for most of the peaks between them. The minor peaks C' and D for the crystalline ASR are also not observed for the amorphous product. This suggests a substantial difference of the atomistic configuration between the crystalline and amorphous regions.

To further identify the atomistic structure, the spectra of the ASR products are compared with the spectra of the reference phases (Figure 3.1d). The spectra of the crystalline ASR products, e.g. ES2_pt3 and Mels1_pt1, resemble the spectrum of shlykovite, instead of the spectrum of mountainite. This strongly suggests that shlykovite is a better structural analogue to the crystalline ASR products from several field sources. On the other hand, the spectra of the amorphous region, e.g. N1_pt6 and ES2_pt7, are highly comparable to that of K_CSH and a reported data of nano-crystalline C-S-H (CSH* [13] in Figure 2d), suggesting that the amorphous ASR product in the cementitious paste are structurally similar to C-S-H. This finding is further confirmed by the K and Na *K*-edge spectra. More details are available in our published work [14].

3.2 Crystal structure refined with XRD data

Based on the observation of micro-XAS study, we then validated the feasibility of solving the crystal structure of the ASR product starting from a shlykovite structure. As shown in Figure 3.2a, the lab-synthesized SKC and SNC yield similar diffraction patterns as shlykovite, despite the difference in the relative intensities of a few peaks. The XRD of the extracted ASR products, e.g. ES1_agg, ES1_pore and Mels_pore, are in general similar to that of the SKC. However, peaks seem broadened and merged with adjacent peaks in the ASR products. The relative intensity of the basal peaks ($1/d < 0.1$ Å^{-1}) for the ASR products and the lab-synthesized samples are significantly smaller than that of shlykovite. This indicates a limited crystallite size perpendicular to the silicate layer, i.e. along the *c*-axis. This is in consistence with the nano-platy morphology of both field ASR samples and lab-synthesized samples.

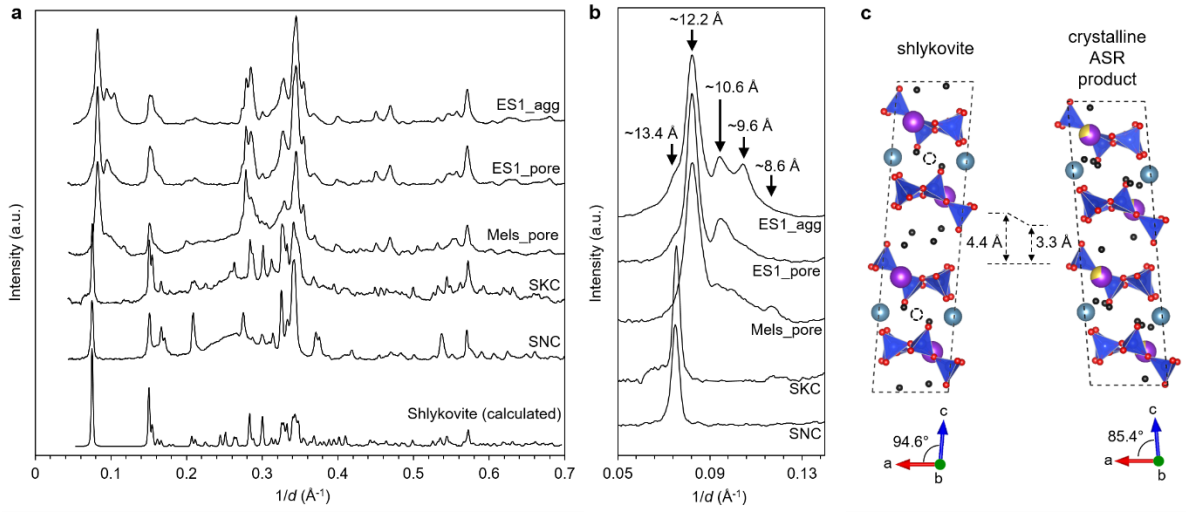

Figure 3.2: XRD data of the extracted crystalline ASR product and the reference phases (a). An enlarged picture of the basal peak regions (b). An illustration of the refined structure for crystalline ASR products (color code following Figure 1), compared with the shlykovite structure. The atomic ratio of Na/K/Ca/Si were refined to fit the data of Mels1 in Table 1. The figures are adapted from [14].

On the other hand, the extracted samples exhibit multiple basal peaks (Figure 3.2b) with basal spacing ranging from ~8.6 to ~13.4 Å, whereas shlykovite, SKC and SNC has only one basal peak at *d*~13.6 Å. This indicates that, although the extracted ASR products may have a similar layer structure as shlykovite, their layer-stacking pattern might be different. For instance, the crystalline ASR products may have different stacking distance (i.e. basal spacing). The variation in basal spacing could be due to the difference in interlayer cation types and contents, as in the case of many clay minerals [15]. Table 2.1 indeed shows that the Na/Si, K/Si and Ca/Si measured from crystalline ASR products may vary in the range of 0.07-0.14, 0.16-0.20 and 0.22-0.24, respectively. On the other hand, temperature has been reported to cause dehydration and shrinkage of the basal spacing of crystalline ASR products [15]. It is also possible that the ASR products has undergone different temperature history and thus different degree of dehydration.

A Rietveld refinement was applied to the XRD of Mels_pore, since it is dominated by one single phase, according to the basal peak. We started from the monoclinic shlykovite structure with a $P2_1/c$ symmetry. We allow three types of parameters to be refined, i.e. 1) the anisotropic crystallite size, 2) the lattice parameters, and 3) the occupancy and content of water molecules in the interlayer and main layer. A satisfactory refinement resulted in *a*, *b*, *c* and *β* to be 6.634(5) Å, 6.513(5) Å, 23.37(3) Å and 85.3(5)°. Compared to the lattice parameters of shlykovite (*a* = 6.4897 Å, *b* = 6.9969 Å, *c* = 26.714 Å and *β* = 94.597°), the unit cell in the field samples is slightly elongated along *a*-axis, but shortened along *b*-axis. The interlayer spacing of the field sample is about 1.1 Å shorter than that of shlykovite. The *β* angle also decreases by ~9.2°. The configurational difference between the crystalline ASR product and shlykovite can be illustrated by a shear glide between the adjacent layers along the *a*-axis, as shown in Figure 3c. The refinement also results in less water in the interlayer and more water in the main layer, compared with the case of shlykovite. This is consistent with the shortened interlayer in the crystalline ASR product. The readers are referred to our published paper for more details of the refinement [14].

3.3 Mechanical properties studied by high-pressure XRD

The intrinsic mechanical property of the crystalline ASR products was studied by high-pressure XRD. Diffractograms of the powder were measured at different pressure values. An example of ES1_agg is given in Figure 3.3a, where the sample was loaded from 0 to 7.5 GPa, and then unloaded to 1.65 GPa. As the applied pressure increases, all diffraction peak moves to the right-hand-side, meaning that the *d*-spacing decreases at elevated pressure.

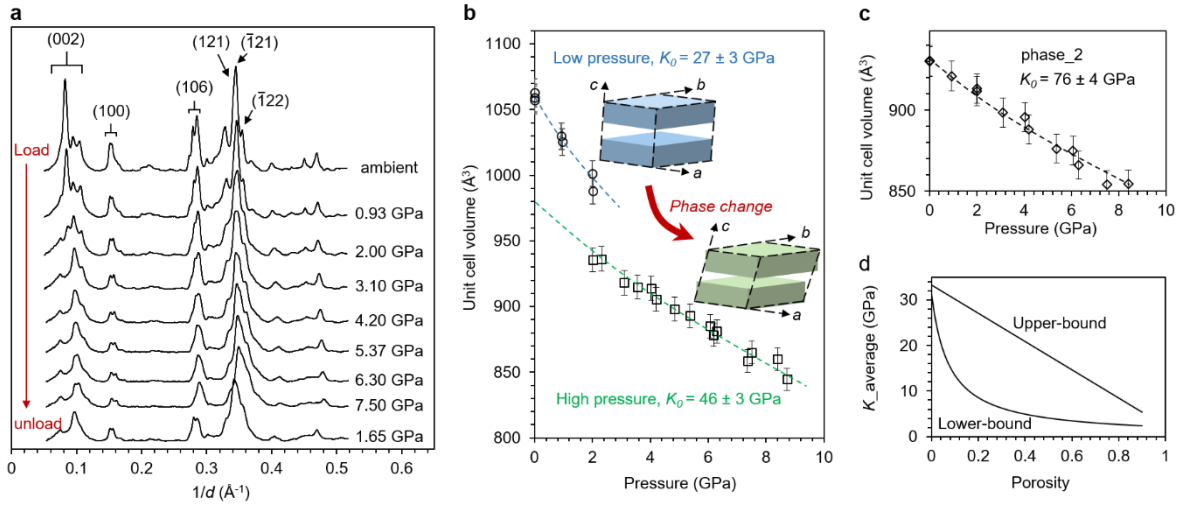

Figure 3.3: Diffractograms of ES1_agg as a function of applied pressure (a). The unit cell volume of the dominant phase (phase_1) in ES1_agg as a function of pressure, from which the bulk modulus can be fitted (b). The unit cell volume – pressure curve of the minor phase (phase_2) in ES1_agg (c). The lower and upper boundary of the averaged bulk modulus of the ASR product as function of porosity, considering a 2:1 mixing ratio of phase_1 and phase_2. The figures are adapted from [17].

At ambient pressure three basal peaks are clearly observed for ES1_agg, with a dominant basal peak at *d*~12.2 Å. The crystal structures corresponding to each basal peak are named phase_1, phase_2

and phase_3. According to the finding in the micro-XAS study and Rietveld refinement, these phases most likely have the same calcium-alkali-silicate layer, but are different in the layer stacking distance. When the pressure reaches 2.0 GPa, the intensity of the dominant basal peak significantly decreases, and is no longer observed when pressure reaches 3.1 GPa. Meanwhile, the intensity of the basal peak of phase_2 suddenly increases when pressure increases from 0.93 GPa to 2.0 and 3.1 GPa. This implies a sudden collapse of the layer stacking of phase_1 at 2.0 GPa, and the resulted stacking distance is close to the basal spacing of phase_2.

The previous Rietveld refinement enabled us to assign the Miller index to each diffraction peaks. Their *d*-spacings can thus be used to calculate the lattice parameters, including the unit cell volume. In Figure 3.3b, the unit cell volume of phase_1 in ES1_agg, ES1_pore and Mels_pore are plotted together as a function of pressure. A clear shift of the trend line is identified at ~2 GPa, corresponding to a sudden change of unit cell volume. Further calculation of lattice parameter suggests this change to be a displacive phase transformation, which takes place by a rapid shortening of the interlayer spacing and a shear glide of adjacent layers (picture insets in Figure 3.3b). The readers are referred to our submitted work for more details [17].

Pressure has been reported to cause the dehydration of crystal structure [18]. Unfortunately, our powder XRD data is not sufficient to validate if this phenomenon drives the phase change of the phase_1 in our ASR samples. Further investigations using high pressure Raman spectroscopy may provide more evidence.

The bulk moduli K_0 are estimated by fitting the volume-pressure data with the 2nd order Birch-Murnaghan equation of state (Eq.1) (Birctt, 1952).

$$P = \frac{3}{2}K_0\left(\left(\frac{V}{V_0}\right)^{-\frac{7}{3}} - \left(\frac{V}{V_0}\right)^{-\frac{5}{3}}\right) \quad (1)$$

The bulk modulus of the phase_1 in crystalline ASR product was fitted to be 27±3 GPa at ambient pressure, and 46±3 GPa after the phase change above 2 GPa. Similarly, the bulk modulus of the phase_2 in crystalline product was fitted to be 76±4 GPa (Figure 4c).

The overall bulk modulus $K_{\_average}$ of the crystalline ASR product in the vein is determined by the mixing ratio of phases that are of different basal spacing and bulk modulus. The void gap between the nano-platelets, i.e. the porosity, also substantially influences $K_{\_average}$. Here, without considering the anisotropy of the nanocrystalline ASR products, an upper and lower bound of $K_{\_average}$ can be readily determined based on the Voigt (Eq.2) and Reuss (Eq.3) assumption, respectively [19].

$$\text{Upper bound: } K_{\_average} = \sum_i f_i * K_i \quad (2)$$

$$\text{Lower bound: } K_{\_average} = 1/\sum_i\left(\frac{f_i}{K_i}\right) \quad (3)$$

Where the f_i and K_i are the volume percentage and the bulk modulus of each phase. Assuming the product vein is filled with phase_1 and phase_2 in a volume ratio of 2:1, the boundary value of $K_{\_average}$ is calculated as a function of porosity according to Eq. 2&3, as shown in Figure 3.3d. For instance, when the porosity of the ASR product vein is 0.2, the overall bulk modulus of the product ranges between 9 and 30 GPa. When the porosity is 0.5, the lower and upper bound becomes 4 and 18 GPa, respectively. This boundary range may be further narrowed if the texture information (orientation distribution) of the ASR nano-platelets are investigated in the future. The existing nano-indentation work reported an elastic modulus between 7 and 9 GPa [20], which is close to the lower bound of our estimation.

4. CONCLUSIONS

In this project we utilized synchrotron-based micro-chemistry and crystallography probes to study the ASR products from real affected concrete and from lab-synthesis. The key conclusions are given as follows. We refer interested readers to our journal publications for more scientific details [12][14][17].

1) Crystalline ASR products are ubiquitously observed in affected concrete. Despite the distinct sources, several crystalline ASR products exhibit highly comparable crystal structure, which is confirmed to highly resemble shlykovite – a natural mineral with monoclinic structure. The amorphous ASR products from several affected concrete are nearly identical, with a structure similar to C-S-H.

2) The crystalline ASR products differ to the natural shlykovite in the stacking behaviour of calcium alkali silicate layer. For instance, the basal spacing in the crystalline product of field samples are variable. The adjacent layers in the crystalline product of field samples may glide along the *b*-axis, resulting in a clear change in the β angle.
3) The studied crystalline ASR products contain multiple phases with different basal spacing. The dominant phase has a bulk modulus of 27±3 GPa. Under hydrostatic compression of ~2 GPa, it transforms to a different polymorph with a bulk modulus of 46±3 GPa. The phases change takes place via a shortening of ~ 1 Å in the interlayer spacing, accompanied by a shear glide of the main layer along both *a*- and *b*-axis. The minor phase has a bulk modulus of 76±4 GPa. It exhibits no phase change during compression to ~8 GPa.

5. REFERENCES

[1] Merz C, Hunkeler F, Griesser A (2006) Schäden durch Alkali-Aggregat-Reaktion an Betonbauten in der Schweiz. UWEK, Forschungsauftrag AGB2001/471, Bericht Nr. 599, Bern.

[2] Cole WF, Lancucki CJ, Sandy MJ (1981) Products formed in an aged concrete. Cem Concr Res 11: 443-454. https://doi.org/10.1016/0008-8846(81)90116-2

[3] De Ceukelaire L (1991) The determination of the most common crystalline alkali-silica reaction product. Mater Struct 24: 169-171. https://doi.org/10.1007/BF02472981

[4] Fernández-Jiménez A, Puertas F (2002) The alkali–silica reaction in alkali-activated granulated slag mortars with reactive aggregate. Cem Concr Res 32: 1019-1024. https://doi.org/10.1016/S0008-8846(01)00745-1

[5] Shi Z, Shi C, Zhao R, Wan S (2015) Comparison of alkali–silica reactions in alkali-activated slag and Portland cement mortars. Mater Struct 48: 743-751. https://doi.org/10.1617/s11527-015-0535-4

[6] Peterson K, Gress D, Van Dam T, Sutter L (2006) Crystallized alkali-silica gel in concrete from the late 1890s. Cem Concr Res 36: 1523-1532. https://doi.org/10.1016/j.cemconres.2006.05.017

[7] Katayama T (2012) Late-expansive ASR in a 30-year old PC structure in eastern Japan, Proceeding of the 14th International Conference on Alkali-Aggregate Reaction (ICAAR), Austin, USA.

[8] Leemann A (2017) Raman microscopy of alkali-silica reaction (ASR) products formed in concrete. Cem Concr Res 102: 41-47. https://doi.org/10.1016/j.cemconres.2017.08.014

[9] Dähn R, Arakcheeva A, Schaub P, Pattison P, Chapuis G, Grolimund D, Wieland E, Leemann A (2016) Application of micro X-ray diffraction to investigate the reaction products formed by the alkali–silica reaction in concrete structures. Cem Concr Res 79: 49-56. https://doi.org/10.1016/j.cemconres.2015.07.012

[10] Lindgård J, Nixon Ph J, Borchers I, Schouenborg B, Wigum BJ, Haugen M, Åkesson U (2011) The EU "PARTNER" project - European standard tests to prevent alkali reactions in aggregates: final results and recommendations. Cem Concr Res 40: 611-635. https://doi.org/10.1016/j.cemconres.2009.09.004

[11] Pekov IV, Zubkova NV, Filinchuk YE, Chukanov NV, Zadov AE, Pushcharovsky DY, Gobechiya ER (2010) Shlykovite KCa[Si4O9(OH)]·3H2O and cryptophyllite K2Ca[Si4O10]·5H2O, new mineral species from the Khibiny alkaline pluton, Kola peninsula, Russia. Geol Ore Deposit 52: 767-777. https://doi.org/10.1134/S1075701510080088

[12] Shi Z, Geng G, Leemann A, Lothenbach B (2019) Synthesis, characterization, and water uptake property of alkali-silica reaction products. Cem Concr Res 121: 58-71. https://doi.org/10.1016/j.cemconres.2019.04.009

[13] Guo X, Wu J, Yiu YM, Hu Y, Zhu YJ, Sham TK (2013) Drug-nanocarrier interaction-tracking the local structure of calcium silicate upon ibuprofen loading with X-ray absorption near edge structure (XANES), Phys. Chem Chem Phys 15: 15033-15040. https://doi.org/10.1039/C3CP50699A

[14] Geng G, Shi Z, Leemann A, Borca C, Huthwelker T, Glazyrin K, Pekov IV, Churakov S, Lothenbach B, Dähn R, Wieland E (2020) Atomistic structure of alkali-silica reaction products refined from X-ray diffraction and micro X-ray absorption data. Cem Concr Res 129: 105958. https://doi.org/10.1016/j.cemconres.2019.105958

[15] Anderson RL, Ratcliffe I, Greenwell HC, Williams, Cliffe S, Coveney PV (2010) Clay swelling-a challenge in the oilfield. Earth-Sci Rev 98: 201-216. https://doi.org/10.1016/j.earscirev.2009.11.003

[16] Davies G, Oberholster RE (1986). The alkali-silica reaction product, a mineralogical and electron microscopic study. In Proceedings of the 8th International Conference on Cement Microscopy, Orlando, USA.

[17] Geng G, Shi Z, Leemann A, Glazyrin K, Kleppe A, Daisenberger D, Churakov S, Lothenbach B, Wieland E, Dähn R. Mechanical behavior and phase change of alkali-silica-reaction products under hydrostatic compression. *Submitted*.

[18] Qin F, Wu X, Qin S, Zhang D, Prakapenka VB, Jacobsen, SD (2019). Pressure-induced dehydration of dioptase: A single-crystal X-ray diffraction and Raman spectroscopy study. Comptes Rendus Geoscience, 351: 121-128.

[19] Li S, Wang G (2008). Introduction to Micromechanics and Nanomechanics. Singapore: World Scientific Publishing Company.

[20] Leemann A, Lura P (2013) E-modulus of the alkali–silica-reaction product determined by micro-indentation. Constr Build Mater 44: 221-227.